Statistical Iteration Reconstruction based on Gaussian Mixture Model for Photon-counting CT

Danyang Li[a], Zheng Duan[a], Dong Zeng[a], Zhaoying Bian[a], and Jianhua Ma[a]

[a]School of Biomedical Engineering, Southern Medical University, Guangzhou 510515, China

ABSTRACT

Photon-counting computed tomography (PCCT) can simultaneously obtain multi-energy data with abundant energy-dependent material-specific information of the scanned object. However, the photon counts in each energy bin are decreased and the collected data suffers from photon starvation effects, which degrades the quality of the reconstructed PCCT images. To solve it, many statistical iteration reconstruction (SIR) methods have been proposed by constructing data-fidelity and prior information terms to suppress noise and remove artifacts. However, most of the current SIR methods assume the noise in PCCT images follows a Gaussian distribution, which deviates the real distribution of the noise in PCCT images. Therefore, we propose a new statistical iteration reconstruction method by considering more complex noise distribution in reality. Specifically, Gaussian mixture model (GMM), which is a universal approximator for any continuous density function, is utilized to model the noise in PCCT images. Moreover, the multi-energy PCCT images are treated as a 3-order tensor which is regularized by three dimensional total variation (3DTV) prior term. Finally, a statistical iteration reconstruction model based on GMM and 3DTV is established for PCCT imaging. For shorten, we call the presented reconstruction model as "GMM-3DTV". We then develop an expectation-maximization (EM) algorithm to solve the presented GMM-3DTV method. Numerical studies demonstrate the improvements of the presented GMM-3DTV method over the competing methods.

Keywords: Photon-counting CT, statistical iteration reconstruction, Gaussian mixture model, 3DTV.

1. INTRODUCTION

Recently, photon-counting computed tomography (PCCT) has been developed in clinics. It utilizes the photon counting detectors (PCDs) to simultaneously count photons in multi-energy bins. By obtaining abundant energy-dependent material-specific information and high contrast-to-noise ratio (CNR) for soft materials, PCCT has the advantages on material decomposition and lesion diagnostic.[1,2]

However, the narrow energy bin receives decreasing photons and the spectral data suffers from serious quantum noise.[3] This challenge significantly degrades the quality of the reconstructed PCCT images in multi-energy bins and effects the imaging performance of PCCT imaging. To obtain high quality PCCT images, several statistical iteration reconstruction (SIR) methods have been exploited. It incorporates the statistical property of X-ray photons and prior information of the desired PCCT images to build reconstruction model with data fidelity and regularization terms, respectively. For examples, Xu *et al.* introduced a statistical interior tomography method with TV regularization to reconstruction PCCT images,[4] Kim *et al.* stacked similar image patches at the same position and utilized a low-rank regularization to suppress image noise.[5] Zhang *et al.* utilized a nonlocal mean regularization of the full-spectrum image to maintain the image details.[6] Yao *et al.* proposed to improve the reconstruction performance by utilizing a nonlocal spectral similarity of a weighted image.[7] Liu *et al.* developed a nonlocal total variation (TV) regularization term to construct the weights from the full-spectrum images.[8] Tao *et al.* utilized the structural redundancy between the base materials and the spectral images to establish a prior-knowledge-aware material decomposition method.[9] Zeng *et al.* analyzed the intrinsic tensor properties of the PCCT images and constructed a full-spectrum-knowledge-aware tensor model for PCCT imaging.[10] These methods have been shown great potential in preserving image structures and suppressing noise. Moreover, deep

Further author information: (Send correspondence to J.M. and Z.B.)
J.M.: E-mail: jhma@smu.edu.cn
Z.B.: E-mail: zybian@smu.edu.cn

7th International Conference on Image Formation in X-Ray Computed Tomography,
edited by Joseph Webster Stayman, Proc. of SPIE Vol. 12304, 123042P
 · 0277-786X · doi: 10.1117/12.2646647

learning (DL) based methods have been utilized in spectral CT. For examples, Li *et al.* constructed a cascade DNN to estimate the high-energy image from low-energy image,[11] and Cong *et al.* estimated the PCCT images from the data of energy-integrating detectors by using DNN based method.[12]

However, most of the current SIR methods assume the noise in PCCT images follows a Gaussian distribution, which deviates the real distribution of the noise in PCCT images. Because the artifacts, which maybe induced by beam hardening effect in lower energy bins or photon starvation effect of high density materials, would complicate the noise distribution in the image and invalidate the performances of the aforementioned SIR methods. In addition, the DL-based methods need a quantity of paired data to train a desired network, and the collection of training data is time-consuming and the clinical PCCT data is hard to be obtained. To solve it, we propose to utilize Gaussian Mixture Model (GMM),[13] which is a universal approximator for any continuous density function, to model the noise in the PCCT images. Moreover, we treat the PCCT images as a 3-order tensor and serve the three dimensional total variation (3DTV)[14] as image prior. Finally, we construct a statistical iteration reconstruction method based on GMM and 3DTV. For shorten, we call the presented reconstruction method as "GMM-3DTV".

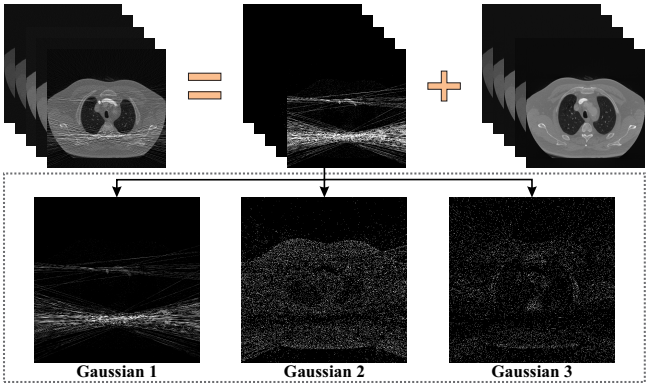

Figure 1. Illustration of the approximated results by the GMM for complex noise in multi-energy bin PCCT images. First row (from left to right): Noisy PCCT images, noise and ground truth. Second row: three noise components of GMM in Bin 1.

In summary, the main contributions of this work are:

- We present a statistical iteration reconstruction method, called GMM-3DTV, by modelling the complex distribution of the noise with GMM and serving the 3DTV as the PCCT image prior.
- Considering the GMM parameters, we also employ an expectation-maximization (EM) algorithm to numerically optimize the presented GMM-3DTV method.
- We evaluate the presented GMM-3DTV on simulated and synthesized clinical data and demonstrate its effectiveness in terms of qualitative and quantitative metrics.

2. METHODS

PCCT receives spectral data among multi-energy bins. Considering the spatial and energy dimensions of the measurements, the 3D PCCT imaging model can be expressed as follows:

$$\mathcal{Y} = \mathcal{A}\mathcal{X}, \tag{1}$$

where $\mathcal{Y} = \{y_n, n \leq N\}$ and $\mathcal{X} = \{x_n, n \leq N\}$ denote the measurements and reconstructed PCCT images among multi-energy bins, respectively. N is the total number of the multi-energy bins. $\mathcal{A}$ is a linear projection operator. It should be note that additional constraints are incorporated to stable the solution of the above model.

Due to the variance of the material attenuations for X-ray along the whole spectrum, the feature of the noise is different among multi-energy bins. Specifically, the reconstructed images in lower bins suffer from strip artifacts due to the beam hardening, and the ones in higher bins are corrupted by the photon starvation induced noise. Therefore, a single Gaussian is no sufficient to approximate the complex noise distribution in the PCCT images.

Fig. 1 shows the noisy PCCT images, noise and ground truth. It can be seen that the PCCT images have multiple modalities of noise, as illustrated by the three Gaussian components in Bin 1, and a simple Gaussian noise model may deviate the real cases. In order to solve the complex noise distribution, we model the noise in the PCCT images as a parametric probability distribution by GMM for more flexibly adapting different cases. Specifically, the noise term ε_n in the nth energy bin is expressed as follows:

$$\varepsilon_n \sim \sum_{k=1}^{K} \pi_{nk} \mathcal{N}\left(\varepsilon_n | \mu_{nk}, \sigma_{nk}^2\right), \tag{2}$$

where π_{nk}, μ_{nk} and σ_{nk}^2 denote the mixture rate, mean and variance values of the kth Gaussian compound in nth energy bin, respectively. In this work, the mean values are set to be zero. K is the total number of Gaussian compounds, and $\sum_{k=1}^{K} \pi_{nk} = 1$.

Considering the sparsity structures and low rank property of the PCCT images, a general 3D total variation (3DTV) term is utilized as the prior, as follows:

$$R_{3DTV}\left(\mathcal{X}\right) = \sum_{m=1}^{3} \|\nabla_m \mathcal{X}\|_1, \tag{3}$$

where ∇_m is different operations along spatial height, width and spectrum modes of $\mathcal{X}$, $\|\cdot\|_1$ is the L_1 norm. Therefore, coupling the GMM approximation for noise and sparse regularization for PCCT images, we can formulate a robust penalized weighted least squares method for PCCT imaging as follows:

$$\begin{aligned} &\min_{\mathcal{X}} \frac{1}{2}\|\mathcal{Y} - \mathcal{A}\mathcal{X}\|_2^2 + \alpha R_{3DTV}\left(\mathcal{X}\right), \\ &s.t.\ \varepsilon_n \sim \sum_{k=1}^{K} \pi_{nk} \mathcal{N}\left(\varepsilon_n | \mu_{nk}, \sigma_{nk}^2\right), n = 1, ..., N, \end{aligned} \tag{4}$$

where α is a hyper-parameter of the image prior term. Simply, we call the above method as "GMM-3DTV" method. Finally, by imposing the negative form of likelihood function of the GMM, Eq. (4) is rewritten as follows:

$$\begin{aligned} \min_{\mathcal{X},\Pi,\Sigma} &\frac{1}{2}\|\mathcal{Y} - \mathcal{A}\mathcal{X}\|_2^2 + \alpha R_{3DTV}\left(\mathcal{X}\right) \\ &- \beta \sum_{n=1}^{N} \log \sum_{k=1}^{K} \pi_{nk} \mathcal{N}\left(\varepsilon_n | 0, \sigma_{nk}^2\right), \end{aligned} \tag{5}$$

where β is the hyper-parameters of GMM likelihood term. $\Pi = \{\pi_{nk}, n \leq N, k \leq K\}$ and $\Sigma = \{\sigma_{nk}^2, n \leq N, k \leq K\}$ are the sets of mixture coefficients and variance values, respectively. Moreover, we adopt an Expectation Maximization (EM) algorithm [15] to iteratively optimize the presented GMM-3DTV method.

The whole EM algorithm for optimizing Eq. (5) can be summarized in Algorithm 1.

3. RESULTS

3.1 Implementation Details

In this work, we compare the presented GMM-3DTV method with the filtered back projection (FBP) method using a ramp filter and a tensor-based dictionary learning regularization (TDL) method. In addition, two more

Algorithm 1: Algorithm for Solving Eq. (5)

Input : The PCCT multi-energy measurements $\mathcal{Y}$, regularized parameters α and β, and stopping criteria ϑ.

Output: Reconstructed PCCT multi-energy images $\mathcal{X}$.

Initialization: $\mathbf{\Pi}, \mathbf{\Sigma}$, GMM number K;

while *not satisfy stopping criteria* ϑ **do**

  E step: calculate the expectation of posterior probability of GMM parameters;

  M step: maximum the augmented Lagrangian function.

end

methods are implemented to investigate different parts of the presented GMM-3DTV method. The one is GMM-based reconstruction model, and the other is 3DTV-based reconstruction model. The images at normal dose serve as the ground truth. Two numerical phantoms are utilized to validate the performance of the presented method. Specifically, XCAT phantom[16] contains alcohol, water, bone and gadolinium, and the synthesized clinical phantom includes water, bone and iodine. The phantoms are scanned under the simulated 120 kVp X-ray spectrum with 1.6 mm Al filtration by SPEKTR toolbox.[17] Five energy bins with equal photon counts are determined by the thresholds: 25, 50, 60, 70 and 85 keV. The PCCT imaging parameters are set as follows: (1) source-to-detector and source-to-center distances are 1040.0 and 570.0 mm, respectively. (2) 1160 projection views are evenly scanned the objections over 360^o. (3) 816 detector channels are placed along the parallel X-ray beam. To generate the noisy projections, Poisson noise is applied into the simulated noise-free projections.

Figure 2. Reconstructed images of the presented and compared methods on XCAT phantom. The display windows from Bin 1 to 5 are [0.00, 0.02], [0.00, 0.010], [0.00, 0.017], [0.00, 0.015] and [0.00, 0.010] mm^{-1}, respectively. Zoomed ROIs indicated by the red boxes are displayed for better visualization.

3.2 Qualitative Analysis

Fig. 2 shows visual comparisons of the presented and compared methods on XCAT phantom. It can be observed that: 1) the FBP method suffers from noise-induced artifacts, and the other methods outperform the FBP method in terms of improving the image quality; 2) the 3DTV-based method suffers from blocky artifacts and the GMM-based method remains producing noisy images; 3) the TDL method smooths the images and enhances the texture of the noise-induced artifacts; 4) the presented GMM-3DTV method better handles the noise-induced artifacts and preserves the image details. Moreover, zoomed in regions-of-interest (ROIs) indicated by the red boxes in each image are illustrated. It can be observed that the presented GMM-3DTV maintains the details of the anatomic structures.

Fig. 3 illustrates the results of different methods on synthesized clinical phantom. Similar with the results on XCAT phantom, the TDL method fails to denoise among the multi-energy bins, the 3DTV induces additional block artifacts for the denoising results, and the GMM-based method hardly removes the noise. On the contrary, the presented GMM-3DTV method can effectively remove the noise-induced artifacts and recover the images details. For better visual inspection, zoomed in ROIs indicated by the blue boxes are shown, which also demonstrates the same conclusion.

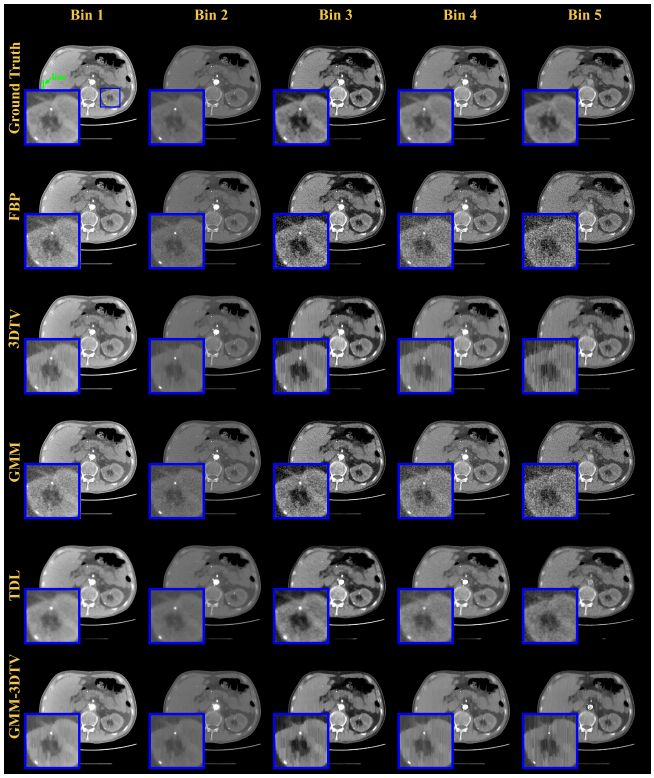

Figure 3. Reconstructed images of the presented and compared methods on synthesized clinical phantom. The display windows from Bin 1 to 5 are [0.007, 0.0105], [0.0032, 0.0072], [0.003, 0.004], [0.0022, 0.0035] and [0.0018, 0.0027] mm^{-1}, respectively. Zoomed ROIs indicated by the blue boxes are displayed for better visualization.

Fig. 4 shows the profiles of different methods on synthesized clinical phantom indicated by the green line in Fig 3. From the results, we can seen that the TDL and 3DTV-based methods produce blurry results, and the GMM-based method fails to suppress the noise. In contrast, the results of the presented GMM-3DTV method are the closest to the ground truth.

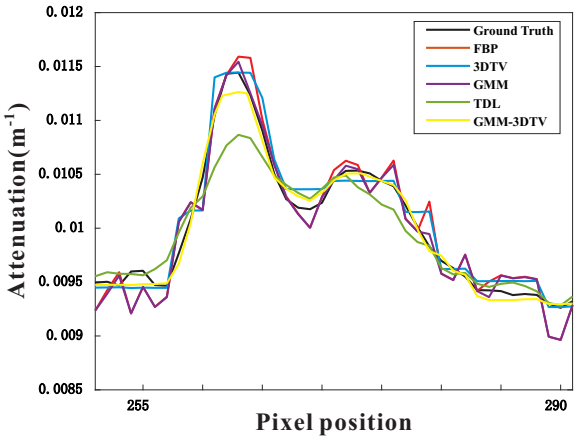

Figure 4. Profiles of the results from different methods on synthesized clinical phantom. The location of the profiles is indicated by the green line in Fig. 3 for each reconstructed images in Bin 1.

3.3 Quantitative Analysis

In this work, root-mean-square-error (RMSE) is calculated to quantify the errors between the ground truth and the results reconstructed by different methods. As shown in Tab. 1 and Tab. 2, the presented GMM-3DTV method achieves consistently better metrics with smallest RMSE on both phantoms. In addition, it can be observed that the reconstruction performance of the presented GMM-3DTV method is significantly heightened by fusing the GMM and 3DTV terms.

Table 1. Quantitative measurements on the reconstruction results on XCAT phantom from the different methods.

	RMSE ($\times 10^{-4}$)
FBP	14.066
3DTV	14.534
GMM	8.957
TDL	5.244
GMM-3DTV	**5.233**

Table 2. Quantitative measurements on the reconstruction results on synthesized clinical phantom from the different methods.

	RMSE ($\times 10^{-5}$)
FBP	11.528
3DTV	4.719
GMM	10.530
TDL	4.076
GMM-3DTV	**3.928**

4. DISCUSSION AND CONCLUSION

Due to the beam-hardening and photon starvation effects, the reconstructed PCCT images suffer from noise-induced artifacts with complex noise distribution in image domain. Most of the SIR methods hardly handle the

artifacts and produce suboptimal results. To address this issue, in this work, we presented a novel SIR PCCT reconstruction method. Specifically, we utilized GMM to approximate the complex noise distribution in the PCCT image domain. Moreover, a 3DTV term, which served as the image prior, was also incorporated into the reconstruction model to encourage structural similarity of the PCCT images along the multi-energy bins. Experiments were conducted to demonstrate the effectiveness of the presented GMM-3DTV method. In the future, clinical and more scene studies would be included to further demonstrate the reconstruction performance of the presented GMM-3DTV method.

ACKNOWLEDGMENTS

This work was supported in part by the NSFC under Grant U21A6005 and Grant U1708261, the National Key R&D Program of China under Grant No. 2020YFA0712200, and Young Talent Support Project of Guangzhou Association for Science and Technology.

REFERENCES

[1] M. J. Willemink, M. Persson, A. Pourmorteza, N. J. Pelc, and D. Fleischmann, "Photon-counting CT: Technical principles and clinical prospects," *Radiology*, vol. 289, no. 2, pp. 293-312, 2018.

[2] K. Taguchi, J. S. Iwanczyk, "Vision 20/20: Single photon counting x-ray detectors in medical imaging," *Medical Physics*, vol. 40, no. 10, p. 100901, 2013.

[3] S. Niu, G. Yu, J. Ma, and J. Wang, "Nonlocal low-rank and sparse matrix decomposition for spectral CT reconstruction,"*Inverse Problems*, vol. 34, no. 2, p. 024003, 2018.

[4] Q. Xu, H. Yu, J. Bennett, P. He, R. Zainon, R. Doesburg, and *et al.*, "Image reconstruction for hybrid true-color micro-CT," *IEEE Transactions on Bio-medical Engineering*, vol. 59, pp. 1711-1719, 2012.

[5] K. Kim *et al.*, "Sparse-view spectral CT reconstruction using spectral patch-based low-rank penalty," *IEEE Transactions on Medical Imaging*, vol. 34, no. 3, pp. 748-760, 2015.

[6] H. Zhang *et al.*, "Iterative reconstruction for dual energy CT with an average image-induced nonlocal means regularization," *Physics in Medicine & Biology*, vol. 62, no. 13, pp. 5556-5574, 2017.

[7] L. Yao *et al.*, "Multi-energy computed tomography reconstruction using a nonlocal spectral similarity model," *Physics in Medicine & Biology*, vol. 64, no. 3, Jan. 2019.

[8] J. Liu, H. Ding, S. Molloi, X. Zhang, and H. Gao, "TICMR: Total image constrained material reconstruction via nonlocal total variation regularization for spectral CT," *IEEE Transactions on Medical Imaging*, vol. 35, no. 12, pp. 2578-2586, 2016.

[9] S. Tao, K. Rajendran, C. H. McCollough, and S. Leng, "Material decomposition with prior knowledge aware iterative denoising (MDPKAID)," *Physics in Medicine & Biology*, vol. 63, no. 19, 2018.

[10] D. Zeng, L. Yao, Y. Ge, S. Li, Q. Xie, H. Zhang, and *et al.*, "Full-spectrum-knowledge-aware tensor model for energy-resolved CT iterative reconstruction," *IEEE Transactions on Medical Imaging*, vol. 39, pp. 2831-2843, 2020.

[11] S. Li *et al.*, "Pseudo dual energy CT imaging using deep learning based framework: Initial study," 2017, *arXiv:1711.07118*. [Online]. Available:http://arxiv.org/abs/1711.07118

[12] W. Cong and G. Wang, "Monochromatic CT image reconstruction from current-integrating data via deep learning," 2017, *arXiv:1710.03784*. [Online]. Available: https://arxiv.org/abs/1710.03784

[13] G. J. McLachlan and K. E. Basford, "Mixture Models: Inference and Applications to Clustering," Marcel Dekker, 1988.

[14] S. Osher, M. Burger, D. Goldfarb, J. Xu, and W. Yin, "An iterative regularization method for total variation-based image restoration," *Multiscale Modeling & Simulation*, vol. 4, no. 2, pp. 460-489, 2005.

[15] A. P. Dempster, N. M. Laird, and D. B. Rubin, "Maximum likelihood from incomplete data via the em algorithm," *Journal of the Royal Statistical Society. Series B (methodological)*, pp. 1-38, 1977

[16] W. P. Segars, G. Sturgeon, S. Mendonca, J. Grimes, and B. M. W. Tsui, "4D XCAT phantom for multimodality imaging research," *Medical Physics.*, vol. 37, no. 9, pp. 4902-4915, Aug. 2010.

[17] J. Punnoose, J. Xu, A. Sisniega, W. Zbijewski, and J. H. Siewerdsen, "Technical note: Spektr 3.0-A computational tool for X-ray spectrum modeling and analysis," *Medical Physics*, vol. 43, no. 8Part1, pp. 4711-4717, 2016.